HAL
open science

Pulsed frequency-shifted feedback laser for laser guide stars: intracavity preamplifier

J. P. Pique, Vincent Fesquet, Sylvie Jacob

To cite this version:

J. P. Pique, Vincent Fesquet, Sylvie Jacob. Pulsed frequency-shifted feedback laser for laser guide stars: intracavity preamplifier. Applied optics, 2011, 50 (33), pp.6294-6301. 10.1364/AO.50.006294 . hal-01115729

HAL Id: hal-01115729

https://hal.science/hal-01115729v1

Submitted on 3 Mar 2015

HAL is a multi-disciplinary open access archive for the deposit and dissemination of scientific research documents, whether they are published or not. The documents may come from teaching and research institutions in France or abroad, or from public or private research centers.

L'archive ouverte pluridisciplinaire **HAL**, est destinée au dépôt et à la diffusion de documents scientifiques de niveau recherche, publiés ou non, émanant des établissements d'enseignement et de recherche français ou étrangers, des laboratoires publics ou privés.

Public Domain

Pulsed Frequency Shifted Feedback Laser for Laser Guide Star: Intra-cavity Preamplifier

Jean-Paul Pique,[1,*] Vincent Fesquet,[2] and Sylvie Jacob,[1]

[1]*Univ. Grenoble 1 / CNRS, LIPhy UMR 5588, Grenoble, F-38041, France*

[2]*Gemini Obs., 670 North A'ohoku Place, Hilo, HI 96720-2700, USA*

[*]*Corresponding author: pique@liphy.ujf-grenoble.fr*

Intensive use of Laser Guide Star (LGS) with the new generation of Extremely Large Telescopes and Hypertelescopes will requires the use of more efficient lasers to surmount the novel limitations and aberrations. The Pulsed Frequency Shifted Feedback (FSF) laser we have developed overcomes the saturation of sodium atoms and solves new problems. This work presents a highly efficient solution for operating pulsed FSF lasers. For the first time, an intra-cavity preamplifier achieves a gain of 10^4 and more than 40 μJ per pulse, with a near diffraction limited beam and without Amplified Spontaneous Emission. Endurance tests have shown that good performance is maintained over several hundred hours.

OCIS codes: 140.3538, 140.3518.

1. Introduction

Progress in laser technology is crucial for the production of Laser Guide Stars (LGS). LGSs, which greatly increase the sky coverage for adaptive optics, are now implemented on

most large telescopes and are expected to play a major role for Extremely Large Telescopes (ELT, TMT …) [1, 2] and hypertelescopes [3]. Yet the nature of the mesospheric sodium layer (thickness about 10% of the Earth-LGS distance, spatial inhomogeneities and temporal fluctuations in the sodium density ...) poses serious problems for ELT [4]. New aberrations, such as spot elongation, focus and tip/tilt errors [5], etc., become dominant. To solve these problems, astronomers have devised highly original solutions [6] that rely on the formation of constellations of several LGSs (up to 22 LGSs for the TMT [7]) launched on the periphery of the primary or secondary mirror and by sodium layer tracking methods. Some of them, however, rely on pulsed lasers operating at repetition rates of the order of kHz. While it is relatively easy to obtain high power pulsed lasers, they are limited by saturation of the sodium atom D_2 transition. To avoid saturation, several alternatives have been considered, such as CW lasers [8], very high repetition rates (~ 80 MHz), mode locked lasers [9] or modeless lasers [10, 11]. A modeless laser can increase the LGS intensity by a factor of 5 with respect to that obtained with a single-mode laser, and by a factor of 2.5 compared to a single-mode laser followed by phase modulation [10]. The work presented here relies on the modeless laser solution. Originally it was supposed that the emission was modeless [12-14] but later investigations showed that a comb of chirped modes exists [15, 16]. The interferometry experiments that have been carried out until now do not, however, prove the existence of a single chirped comb. It is quite possible that many chirped combs coexist with no phase relationship between them, since all spontaneous photons can be amplified, unlike conventional lasers. For LGS, in all cases, the main result is that modeless lasers can excite all the velocity classes of the sodium atoms, thus leading to de-saturation of a given class [10]. The modeless laser is now more commonly referred to as the Frequency Shifted Feedback (FSF) laser.

FSF lasers described in the literature usually operate in continuous wave (CW) mode. It has been shown that a pulsed pumped preamplifier can be introduced into a CW dye laser cavity. 3μJ per pulse has been demonstrated [17]. Our experiments have shown that this energy is insufficient for injecting into an amplifier to produce a laser power compatible with LGS characteristics. In this work we report solutions for enhancing the energy of an intra-cavity pulsed pumped preamplifier to nearly 40 μJ with a TM_{00} spatial mode and a single spectral line that is adjusted to the excitation of the D_2 line of sodium atom. Section 2 describes the FSF laser cavity with its intra-cavity pulsed preamplifier. Section 3 provides a unified code that takes into account the CW and pulsed gain media, as well as spectral and temporal evolution. This code has been of great help in achieving this technological advance. In section 4 we discuss the experimental and theoretical results. This work corresponds to the first stage of the all-optical FSF laser channel that we are developing for CFHT-Lsp_On-sky Experiment (CLOE) project [18]. It will be followed by a single amplifier stage.

2. FSF oscillator-preamplifier set-up

The pulsed FSF laser diagram with its intra-cavity preamplifier (ICPA) is depicted in Figure 1. The diagram is similar to Figure 2 of reference [10]. But in reference [10] we have not studied, experimentally or theoretically, the pulsed intra-cavity preamplifier, only the CW pumping was studied and described. This is what we do primarily in the present article. Moreover, in this article, the preamplifier is not a dye-jet but a dye-cell.

The wavelength of the sodium D_2 line and the particular operation of the laser at present require the use of dyes. The laser cavity consists of two dye amplifier media. One dye (J) is pumped by a CW frequency doubled VANADATE laser (VERDI/Coherent) and the other (C) is

pumped by a pulsed frequency doubled YAG laser operating at a repetition rate of 10 kHz with pulse duration 65 ns (Navigator II/Spectra Physics). The first amplifier medium is a high-precision dye jet (Radiant Dye Laser) and the second is a specially designed quartz dye cell (Hellma). The jet and the cell are positioned at the Brewster angle and are respectively 0.1 mm and 2 mm thick. They are quasi-longitudinally pumped.

It is well known that the gain spectra of dyes are frequency shifted when they are pumped continuously or pulsed. To work optimally at 589 nm, we used Rhodamine 6G (R6G, Exciton) for the jet and Pyrromethene 597 (PM597, Exciton) for the cell, dissolved respectively in ethylene glycol (1.3 mM) and ethanol (0.1 mM). R6G is known to be one of the best dyes with a very long lifetime. The performance of PM597 is excellent, but its lifetime, which did not exceed 10 hours, is insufficient for our purpose. The oxygen triplet $^3O_2$, dissolved in ethanol, reacts with PM597 molecules, which are brought by the intersystem crossing interaction in the triplet state to form singlet oxygen $^1O_2$. The highly reactive $^1O_2$ molecule destroys the ground state PM597 molecules [19]. To address this problem, we added an anti-oxidant (DABCO, 10 mM), which quenches $^1O_2$ very efficiently without affecting the gain of PM597. This increases the lifetime of the ethanol-PM597 solution by an order of magnitude. The result is that by using the maximum pump energy available to us (~ 450 μJ), the output power performance is maintained for several hundred hours.

The laser cavity is similar to that described in references [10, 17]. It consists of the mirrors M_1, M_2 and M_3, the radii of curvature of which are respectively 10 cm, 7.5 cm and infinity. The acousto-optic shifter (AO) operates at an acoustic frequency of 35 MHz and an intra-cavity efficiency of 97%. The cavity is closed on the first diffraction order of the AO. The reflectance of the output mirror M_3 was adjusted to 83% in order to optimize the pulsed intensity.

A three-quartz-plate Lyot-filter (Lyot) and an etalon (E, CVI Melles Griot) are the only selective elements of the cavity. The AO also acts as a broadband filter through the acoustic grazing that is generated. For optimum spectral narrowing, the etalon was placed next to the output mirror M_3 in the Rayleigh range. The etalon has a free spectral range of 400 GHz and a reflection coefficient of 40% on each side. This arrangement yields a single line. This is important because spurious spectral lines of very low intensity will be over-amplified by the last amplifier stage, leading to a multi-line spectrum.

The cell and its pumping system are dominant factors for the efficiency of the ICPA. A cell of cross-section 2×10 mm and a dye circulator was specially designed to yield a high flux (imposed by the high repetition rate of 10 kHz) while remaining laminar. The resulting renewal factor of the dye is 2.5 for an intra-cavity beam diameter of 500 µm. For better reliability, the cell position is adjustable whereas the beam direction remains fixed. To homogenize the longitudinal gain in the cell, the pump beam is split into two beams in order to pump the cell at both ends. This quasi-longitudinal gain pumping in X shape has proven to be highly efficient. The temperature of the dye is stabilized at about 15 °C. This arrangement does not degrade the well known L shape cavity spatial mode, which remains close to TM_{00}. We have measured a M^2 of about 1.1.

3. FSF oscillator-preamplifier Model

The emission characteristics of the FSF laser change considerably from that of conventional lasers. A FSF laser intra-cavity optical wave ν_0 is shifted to $\nu_0+2\nu_{AO}$ after a round trip through the AO shifter, where ν_{AO} denotes the frequency of the corresponding acoustic

wave. This continuous change in frequency disturbs constructive interference of the fixed modes in a conventional laser.

In addition a CW and a pulsed field coexist in the laser cavity described above. To model this system, a simple assumption would be that the CW field, which lasts almost 100 µs, prepares the spectrum and then is amplified without modification during the gain in the cell. The first CW phase could be determined using the stationary model developed in reference [10]. The second pulsed phase could then be described by the well-known temporal rate equations of an amplifier using as initial conditions the final photon density of the preceding CW phase, as was done in Reference [17]. However, the pulse duration of the preamplifier is long enough for dozens of round trips during the second pulsed phase. Strictly speaking, therefore, we cannot consider the temporal and spectral variables to be separated during the amplification phase. For this reason we preferred to develop a new single model that takes into consideration both amplifying media. We use the algorithm of Spellpflug [20], which includes time and spectral variables.

This algorithm consists in dividing the spectral range of integration $\Delta\nu$ into K bins and, for each spectral bin, propagating the well-known rate equations during the round trip i. For the following $i+1$th pass, all frequencies are then shifted by the quantity $2\nu_{AO}$ and the integration is reiterated using the initial conditions of the preceding passage i. Compared to the Spellpflug algorithm, we add the missing closure conditions (which were not necessary in their case) and we introduce both the CW and pulsed pumped amplifying media, R6G and PM597 respectively. The computation time is much longer and requires more memory than the method described in the previous paragraph, but poses no particular problem. At each round trip $K+4$ differential equations must be integrated. The integration range depends on the characteristics of selective elements of the cavity. It is, in principle, equal to the pulse period (typically 100 µs) but can be

reduced if a steady state is reached before the arrival of the pulse, and if it covers both pulsed and CW regimes. In the case of dyes, the integration step must be short enough (~ 300ps) for the transients to be calculated correctly. Unfortunately, this algorithm does not allow the use of an adaptive step that would accelerate the calculations.

The differential equations for the jet and the cell populations N (subscripts j and c respectively for jet and cell, subscripts 1 and 2 for ground and excited levels), taking into account absorption, spontaneous emission, stimulated emission and gain saturation, are

$$\frac{dN_1^j(t)}{dt} = (\exp(-\sigma_p^j N_1^j(t)/\pi w_j^{\,2}) - 1)\frac{\lambda_p^j}{hc}P_{cw} + \frac{N_2^j(t)}{\tau_j} + \\ + \frac{N_2^j(t)}{\pi w_j^{\,2}}\frac{\sigma_l^j}{\tau_{RT}}\int_{-\frac{\Delta\nu}{2}}^{\frac{\Delta\nu}{2}} n(\nu,t)d\nu \tag{1}$$

$$\frac{dN_2^j(t)}{dt} = -\frac{dN_1^j(t)}{dt} \tag{2}$$

$$\frac{dN_1^c(t)}{dt} = (\exp(-\sigma_p^c N_1^c(t)/\pi w_c^{\,2}) - 1)\frac{\lambda_p^c}{hc}P_p(t) + \frac{N_2^c(t)}{\tau_c} + \\ + \frac{N_2^c(t)}{\pi w_c^{\,2}}\frac{\sigma_l^c}{\tau_{RT}}\int_{-\frac{\Delta\nu}{2}}^{\frac{\Delta\nu}{2}} n(\nu,t)d\nu \tag{3}$$

$$\frac{dN_2^c(t)}{dt} = -\frac{dN_1^c(t)}{dt} \tag{4}$$

σ_p^j and σ_p^c are the absorption cross sections of R6G and PM597 at the pump laser wavelengths λ_p^j and λ_p^c, σ_l^j, σ_l^c are the laser emission cross sections, τ_j and τ_c the radiative lifetimes of excited levels, w_j and w_c the pump waists and τ_{RT} the round trip time of the cavity. P_{CW} and P_p are the

CW and pulsed pump powers absorbed in the jet and the cell respectively. P_{CW} is independent of time and P_p is assumed to be Gaussian with a width Δt_p:

$$P_p(t) = \frac{E_p}{\Delta t_p}\sqrt{\frac{2\log(4)}{\pi}}\exp(-2\log(4)(\frac{t-t_p}{\Delta t_p})^2) \tag{5}$$

where E_p is the pump pulse energy.

The spectral range of integration $\Delta\nu$ is divided into K bins of frequency ν. The K differential equations of the intra-cavity photon density $n(\nu,t)$ are

$$\begin{aligned}\frac{\delta n(\nu,t)}{\delta t} = \frac{n(\nu,t)}{\tau_{RT}}(\frac{\sigma_l^j}{\pi w_j^{\,2}}N_2^j(t) + \frac{\sigma_l^c}{\pi w_c^{\,2}}N_2^c(t) - \gamma(\nu)) \\ + \frac{\sigma_l^j}{\pi w_j^{\,2}}N_2^j(t) + \frac{\sigma_l^c}{\pi w_c^{\,2}}N_2^c(t)\end{aligned} \tag{6}$$

$\gamma(\nu)$ is the sum of the transmission losses of all intra-cavity elements consisting of output mirror, AO, Lyot filter, etalon and various parasitic losses (imperfections, scattering ...) [10].

$$\gamma(\nu) = \frac{1}{\tau_{RT}}(T + 2\frac{\pi\nu}{\Delta\nu_{AO}} + 2(\frac{\pi\nu}{\Delta\nu_{Lyot}})^2 + 2\log(1+\frac{4R}{1-R^2}\sin^2(\pi\frac{\nu}{FSR})) + D) \tag{7}$$

T is the output mirror transmission, $\Delta\nu_{AO}$ and $\Delta\nu_{Lyot}$ the spectral bandwidths of the AO and Lyot filter, FSR the free spectral range of the etalon and D additional losses.

The numerical integration of differential equations was performed on the LIPhy Airelle-cluster (84 cpus, 184 GB RAM). The integration time step δt is considered as constant and taken to be a submultiple of the exact cavity round trip time $\tau_{RT} = m\delta t$. The value of m must satisfy the convergence criterion of the differential system.

The results presented below were obtained with the parameters (ICPA, output mirror, etalon ...) listed in Table 1. All other parameters (jet, selective elements ...) are taken from reference [10].

Parameter	Value
ν_{AO}	35 MHz
w_c	250 µm
PM597 concentration	0.1 mM
R6G concentration	1.3 mM
τ_c	3.7 ns
T	17%
R	45%
FSR	400 GHz
Δt_p	65 ns

Table 1. Parameters used in the model.

4. Results and discussion

To our knowledge, pulsed preamplifiers have not previously been inserted into the FSF laser cavity. The suddenness of the introduction of the pulsed regime could profoundly disturb the operation of the FSF laser. This made it necessary to undertake a detailed experimental study, the results of which can be compared to the model. More particularly, in order to optimize the LGS flux, it is important to ensure that the pulse maintains the same spectral properties as defined in the initial goal.

A. Temporal dynamics

Figure 2(a) shows the change with time of the output intensity measured, with a fast photodiode (PD). The average pump powers $\overline{P_p}$ and P_{CW} are set to 5.3 W and 3.45 W respectively. Before the ICPA pump pulse, the output intensity is constant on average. The output pulse then arrives with a delay of 20-25 ns with respect to the pump pulse. This delay corresponds to the build-up of the ICPA. The output pulse length is therefore shorter than that of the pump (~ 65 ns). In the case shown in Fig. 2(b) it is approximately 40 ns. Then, immediately after extinction of the pump pulse, lasing switches off for about 1.5 µs. The continuous phase resumes after this hole and stabilizes after relaxation oscillations, the period of which, surprisingly, is about 1.4 microseconds. We discuss these relaxation oscillations below. The hole corresponds to dye bleaching. At the first round trip of the pulse into the jet, where the waist is only 20 microns, the power density is huge and the bleaching effect dramatically decreases the R6G jet gain below unity. The CW field builds up again after renewal of dye molecules. The intensity then oscillates for almost 5 microseconds and is re-stabilized, typically about 10 microseconds after the pump pulse. It is clear therefore that this particular dynamics limits the repetition rate of the intra-cavity preamplifier to about 100 kHz. However the renewal rate of the dye molecules between two pulses is a more restrictive limitation. In our experience, a repetition rate below 30 kHz is a good compromise. Figures 2(c) and 2(d) show the results of the calculation. The whole of the dynamics, including relaxation oscillations, is well described by the model described above. Only the renewal time of the dye molecules is not included in the model.

Figure 3 shows the calculated and experimental output power P_{out} when the laser operates only in CW ($P_{cw}=3.45$ *W and* $\overline{P_p}=0$) and when the RF power of the AO is gated. The regime of

relaxation oscillations we observed, of the order of a few microseconds, which is standard for solid state amplifying media of class B (upper-state lifetime greater than cavity damping time), is unusual for a conventional dye laser, which is generally of class A, with a fast exponential relaxation to the steady state.

In the case of a single-mode laser, the relaxation frequency is written as:

$$F_{relax} = \frac{1}{2\pi}\sqrt{\frac{\gamma(r-1)}{\tau_{RT}\tau_g} - \left(\frac{r}{2\tau_g}\right)^2} \tag{7}$$

where r is the so-called pump parameter, which is the ratio of pump power P_{CW} to threshold pump power P_{cw}^{th}. τ_g is the upper-state lifetime of the gain medium. With the parameters used above (γ~25%, P_{CW}=3.45 W, P_{cw}^{th}~2 W, τ_{RT}=3.5 ns), τ_g is about 3 microseconds, which is indeed too long for a dye amplifying medium. Strictly speaking, Eq. (7) does not apply to FSF lasers. In particular, the value of the equivalent pump parameter r is very different from that calculated by putting all the power into a single mode and using the threshold of a conventional laser. In the case of the FSF laser, this threshold is difficult to define because the curve of the output power versus pump power exhibits a second order rather than a first order transition [10]. This is the modeless aspect, which explains the phenomenon of microsecond relaxation oscillations, and which is very well described by the photon density model developed earlier (see Fig. 3).

B. Efficiency

Pulse energies E_{out} of almost 40 μJ with pulse duration $\Delta\tau_{out}$ of 40 ns have been obtained, for the first time, using an intracavity preamplifier. Figure 4(c) shows the dependence of E_{out} on the pump energy E_p absorbed into the cell. To eliminate the CW intensity, the output energy is measured using a boxcar that gates the pulse energy and which is calibrated appropriately. The pump power P_{CW} is set at 3.45 W and the pump energy E_p varies from 0 to 450 μJ. The pumping

threshold is about 100 μJ. This relatively high threshold, mainly due to the first order AO loss, is compensated by a good slope efficiency of 12.3%. The measured amplification gain, defined as the ratio of the output energy E_{out} to the CW energy just prior to amplification for the same period $\Delta\tau_{out}$, was about 10^4. This high gain is usually difficult to obtain with an extra-cavity preamplifier. Moreover the output beam of ICPA has many other benefits, namely the absence of ASE (Amplified Spontaneous Emission), the diffraction limited TM_{00} mode of the cavity, and self-alignment.

The energy per pulse E_{out} is calculated from the formula:

$$E_{out} = \frac{hc}{\lambda_l}\frac{T}{2}\pi w_m^{\ 2}\int_{-2\Delta\tau_{out}}^{2\Delta\tau_{out}}\int n(\nu,t)dtd\nu \tag{8}$$

T denotes the output mirror transmission and w_m the output beam waist. The integration is restricted to the duration of the pulse where the contribution of the CW energy is negligible. The theoretical dependence of E_{out} on E_p (Fig. 4(a)) is in very good agreement with experiment. Figure 4(b) and 4(d) show the dependence on E_p of the theoretical and experimental output line-width $\Delta\tau_{out}$. As can be seen, $\Delta\tau_{out}$ reaches an asymptotic value above a pump energy ~200 μJ.

Figure 4(a) demonstrates that we can attain even greater pulse energies. The density of pump power applied to the cell is, however, limited by a marking phenomenon that occurs at the internal liquid-glass interface. Although the dye flow is laminar and the velocity at the center of the cell is large enough, the velocity of the dye solution vanishes at the interface. On the inner faces, multi-photon phenomena are then expected to dissociate the PM597 molecules when the energy density exceeds a value that we have experimentally estimated to be about 0.1 J/cm^2. The use of a jet may cure this problem, but a millimeter-sized jet of good quality has not yet been constructed.

The output mirror reflectance is optimized to yield the highest pulsed energy. The best result was obtained for a reflectance of 83% at 589 nm. This optimization is made at the expense of the CW field, which is characterized by a higher threshold (~ 2W) and relaxation oscillations. To maximize the pulse energy, the pump power P_{CW} can also be adjusted. The shapes of experimental and theoretical curves of figure 5 show good agreement. As noted above, however, the theoretical maximum is higher than that measured experimentally.

C. Spectral properties

Regarding the ICPA of our pulsed FSF laser, the first fundamental question that arises is whether the line-width is conserved during the pulsed amplification. The laser line is analyzed with a home-made scanning plane-plane Fabry-Perrot (FP) with a 33.4 GHz free spectral range and quality factor 200. A boxcar is used to measure the line-width during the pulse. Figure 6 plots the experimental and theoretical line-width $\Delta\nu_{out}$ (FWHM) versus the pump energy E_p using the intra-cavity etalon of 400 GHz free spectral range and a reflection coefficient of 40% at 589 nm.

The model shows no dependence of the line-width on the pump energy, with a value that is close to the experimental measurement. Given the hyperfine structure of 1.77 GHz and the Doppler effect of the sodium atom in the mesosphere, simulations have shown [21] that an ideal line-width is 2.8 GHz. Within the model introduced above we calculate that an etalon of equivalent free spectral range, but with a reflection coefficient of 70% on both sides, should be perfectly appropriate for LGS application.

Another fundamental question is whether the "modeless" or "chirped mode" character is preserved during the pulse. A widely used picture [22] is to consider that a FSF laser spectrum consists of a comb of modes that chirp linearly with time. The chirp speed of our FSF laser is

very fast (about 20 MHz per nanosecond). Such a laser beam injected into a Michelson interferometer exhibits RF beat frequencies at the output of the interferometer:

$$\nu_{RF}^{m} = \nu_0 (m \pm \frac{4\nu_{AO}}{c} z) \tag{9}$$

z is the optical path difference of the two arms of the Michelson interferometer (~ 80 cm in this case), m is an integer and $\nu_0 = 1/\tau_{RT}$ the free spectral range of the laser cavity. These frequencies are found easily through the Fourier transform of the output intensity of the interferometer.

Figure 7 demonstrates these RF frequencies during the pulse of the ICPA. The attenuation above 300 MHz corresponds to the bandwidth of the oscilloscope. Note the recurrence of the free spectral range ν_0 of the laser cavity surrounded by two satellites separated by a well-defined frequency difference $\delta\nu = 4\nu_{AO} \frac{z}{c\tau_{RT}} \approx 106\,MHz$. The existence of these satellites provides a means for ranging measurements with high accuracy [22]. The RF beats are, of course, also observed during time intervals where the laser functions in CW. They are, however, less marked in the area where the initial relaxation oscillations are observed (see Fig. 3). The laser pulse generated by ICPA has therefore a chirped spectrum, which is not surprising, but deserved to be verified.

V Conclusion

In order to produce usable LGSs for new generation ELTs and hypertelescopes, lasers must be more efficient to overcome the new limitations and aberrations. We believe that the high power pulsed FSF laser we are developing in the framework of CLOE project will solve a

number of these constraints. In this work we show the first step: a large energy per pulse is produced on the oscillator-preamplifier part of the laser channel.

The initial advantage of our FSF laser was to solve the problem of saturation of the D_2 transition of atomic sodium. The advances outlined in this paper were greatly facilitated by the code we developed, which is in very good agreement with experimental results. We have shown that the use of an intra-cavity preamplifier with a simple assembly provides more than 40 μJ per pulse. A single intra-cavity etalon enables the laser line-width to be matched to the Doppler-Hyperfine sodium line. A precise mechanical mount, fixed to the Invar rod that maintains the stability of the cavity, can be adjusted precisely to the sodium line. In an air-conditioned room, this passive adjustment remains stable for several days. We have also shown that the use of an anti-oxidant in the solution of PM597 allows the power performance to be maintained over several hundred hours.

Moreover, our all-optical laser has no active electronic feedback, in particular with respect to the wavelength. This provides greater reliability. Furthermore, the regenerative process in the cavity eliminates any ASE, which is broadband and constitutes a major problem with extra-cavity preamplifiers. We could not measure the ASE since it was too low. Note also that the proper use of quasi-longitudinal pumping in the ICPA preserves the mode of the cavity which is close to TM_{00}. The figure of merit of an LGS is the ratio of the return flux to the area of the fluorescence spot. Then, it is clear that a laser beam at the diffraction limit, correctly projected into the mesosphere, will achieve an even better figure of merit [23].

We are currently developing the final amplifier stage in order to raise the energy to 2-3 mJ per pulse with a repetition rate of about 10 kHz while maintaining the optical quality of the beam and compactness.

Acknowledgments

We thank the LIPhy laboratory, the INP and INSU institutes of the CNRS and the CFHT for their constant encouragement and funding in this project. We also thank the Computing Services and the Machine Shop of the LIPhy respectively for helping us to implement our simulation program on the Airelle-cluster and for making the delicate part of the mechanics of the laser. The authors are very grateful to E. Geissler for his contribution in reading the draft.

References

1. J. Nelson, and G.H. Sanders, "The status of the Thirty Meter Telescope project," Proc. SPIE **7012**, 70121A (2008).
2. R. Gilmozzi, and J. Spyromilio, "The 42m European ELT: status," Proc. SPIE **7012**, 701219 (2008).
3. A. Labeyrie, H. Le Coroller, and J. Dejonghe, "Steps toward hypertelescopes on Earth and in space," Proc. SPIE **7013**, 70133J (2008).
4. T. Pfrommer, and P. Hickson, "High-resolution lidar observations of mesospheric sodium and implications for adaptive optics," J. Opt. Soc. Am. A **27**, 97-105 (2010).
5. G. Herriot, P. Hickson, E. Ellerbroek, J.P. Véran, C.Y. She, R. Clare, and D. Looze, "Focus errors from tracking sodium layer altitude variations with laser guide star adaptive optics for the Thirty Meter Telescope," Proc. SPIE **6272**, 62721I (2006).

6. O. Lardière, R. Conan, R. Clare, C. Bradley, and N. Hubin, “Performance comparison of centroiding algorithms for laser guide star wavefront sensing with extremely large telescopes,” Appl. Opt. **49**, G78-G94 (2010).
7. C. Boyer, B. Ellerbroek, L. Gilles, and L. Wang, “The TMT Laser Guide Star Facility,” in Proceedings of 1st AO4ELT conference on Adaptive Optics for Extremely Large Telescopes, (EDP Sciences, 2010), 04004-pp. 1-6.
8. D.B. Calia, W. Hackenberg, S. Chernikov, Y. Feng, and L. Taylor, “AFIRE: fiber Raman laser for laser guide star adaptive optics,” Proc. SPIE **6272**, 62721M (2006).
9. C. d'Orgeville, F. Daruich, G. Arriagada, M. Bec, M. Boccas, S. Bombino, C. Carter, C. Cavedoni, F. Collao, P. Collins, E. James, S. Karewicz, M. Lazo, D. Maltes, R. Mouser, G. Perez, F. Rigaut, R. Rojas, M. Sheehan, G. Trancho, V. Vergara, and T. Vucina, “The Gemini South MCAO laser guide star facility: getting ready for first light,” Proc. SPIE **7015**, 70152P (2008).
10. J-P. Pique, and S. Farinotti, “Efficient modeless laser for a mesospheric sodium laser guide star,” J. Opt. Soc. Am. B **20**, 2093-2101 (2003).
11. J-P. Pique, I.C. Moldovan, and V. Fesquet, “Concept for polychromatique laser guide star: one-photon excitation of the 4P3/2 level of a sodium atom,” J. Opt. Soc. Am. A **23**, 2817-2828 (2006).
12. F.V. Kowalski, P. D. Halle, and, S. J. Shattil, “Broadband Continuous-Wave Laser,” Opt. Lett. **13**, 622-624 (1988).
13. I. C. Littler, S. Balle, and K. Bergmann, “Continuous-Wave Laser Without Frequency-Domain-Mode Structure: Investigation of Emission Properties and Buildup Dynamic,” J. Opt. Soc. Am. B **8**, 1412-1420 (1991).

14. I. C. Littler, and J. H. Eschner, “The CW modeless Laser: Model Calculation of en Active Feedback Cavity,” Opt. Comm. **87**, 44-52 (1992).

15. K. Nakamura, F. Abe, K. Kasahara, T. Hara, M. Sato, and H. Ito, “Spectral Characteristics of an All Solid-State Frequency-Shifted Feedback Laser,” IEEE J. Quant. Elect. **33**, 103-111 (1997).

16. K. Nakamura, T. Miyahara, and H. Ito, “Observation of Highly Phase-Correlated Chirped Frequency Comb Output from a Frequency-Shifted Feedback Laser,” App. Phys. Lett. **72**, 2631-2633 (1998).

17. V. Fesquet, J-P. Pique, I. Courtillot, and I. C. Moldovan, “Intracavity preamplifier of modeless laser,” in Proceeding of IEEE Conference on Lasers and Electro-Optics Europe, (IEEE, 2005), pp. 187.

18. O. Lai, C. Veillet, D. Salmon, K. Ho, M. R. Baril, G. A. Barrick, J. Thomas, D. Teeple, T. Benedict, J-P. Pique, and H. de Chatellus, “VASAO: visible all sky adaptive optics: a new adaptive optics concept for CFHT,” Proc. SPIE **7015**, 701543 (2008).

19. W. N. Sisk, and W. Sanders, “The concentration dependence of the normalized photostability of 1,3,5,7,8-pentamethyl-2,6-di-t-butylpyrromethene-difluoroborate complex (PM-597) methanol solutions,” J. Photochem. Photobio. A, **167**, 185-189 (2004).

20. M. Stellpflug, G. Bonnet, B. W. Shore, and K. Bergmann, “Dynamics of frequency shifted feedback lasers: simulation studies,” Opt. Express **11**, 2060-2080 (2003).

21. I. C. Moldovan, V. Fesquet, F. Marc, H. Guillet de Chatellus, and JP. Pique, “Sodium UV modeless laser excitation for PLGS,” Ann. Phys. Fr. **32**, 91–93 (2007).

22. K. Nakamura, T. Hara, M. Yoshida, T. Miyahara, and H. Ito, “Optical Frequency Domain Ranging by a Frequency-Shifted Feedback Laser,” IEEE J. Quant. Elect. **36**, 305-315 (2000).

23. F. Marc, H. Guillet de Chetellus, and J-P. Pique, “Effects of laser beam propagation and saturation on the spatial shape of sodium laser guide stars,” Optics Express **17**, 4920-4931 (2008).

Table captions

1. Table 1. Parameters used in the model.

Figure captions

1. Fig. 1. Pulsed Frequency Shifted Feedback Laser set-up. J, R6G jet; C, PM597 cell; M_1, M_2, M_3, cavity mirrors; AO, acousto-optic frequency shifter; Lyot, Lyot filter; E, etalon; VERDI, CW 532 nm pump; NAVIGATOR, pulsed 532 nm pump; PD, high speed photodiode; FP, Fabry-Perot analyzer; Na, sodium oven; W-meter, wave meter. For characteristics see text.
2. Fig. 2. Time evolution of the output power of the FSF laser with its intra-cavity pulsed preamplifier. (a) and (b) experiment. (c) and (d) theory. Time zooms (b) and (d) show pulse-widths of about 40 ns. For the relaxation oscillations in (a) and (c) see Fig. 3 and text. Note the ~1.5 μs bleaching time hole of experiment (a), which is not included in the model (c).
3. Fig. 3. (Color online) Build-up of the CW laser power just after the AO-RF power is turned on. (a) experiment, (b) theory and (c) RF power gate. Relaxation oscillations of ~2 μs are well described by the FSF model.
4. Fig. 4. (Color online) ICPA output pulse energy and output pulse-width versus pump energy. (a) and (b) theory, (c) and (d) experiment. The pump threshold is ~100 μJ and the slope efficiency 12.3%. Above pump energy ~200 μJ, the output energy increases linearly and the pulse-width is approximately constant.
5. Fig. 5. (Color online) Output pulse energy versus jet CW pump power. (a) theory and (b) experiment. See text.
6. Fig. 6. (Color online) Line-width versus ICPA pump energy. (a) theory and (b) experiment, in good agreement, show no dependence of the line-width on pump energy.
7. Fig.7. The RF spectrum of the Michelson interferometer output signal for the distance z ~ 80 cm. ν_0 is the free spectral range of the laser cavity. The beat frequency $\delta\nu$ is about 106 MHz.

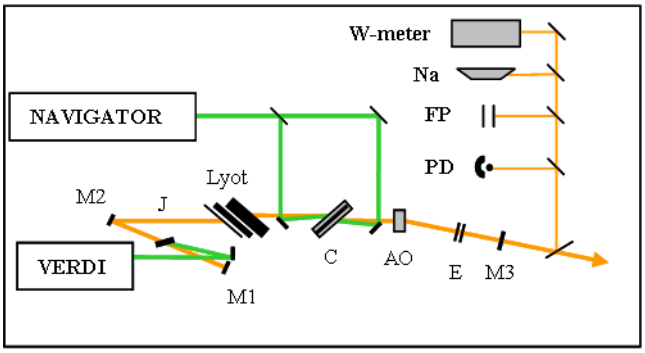

Fig. 1

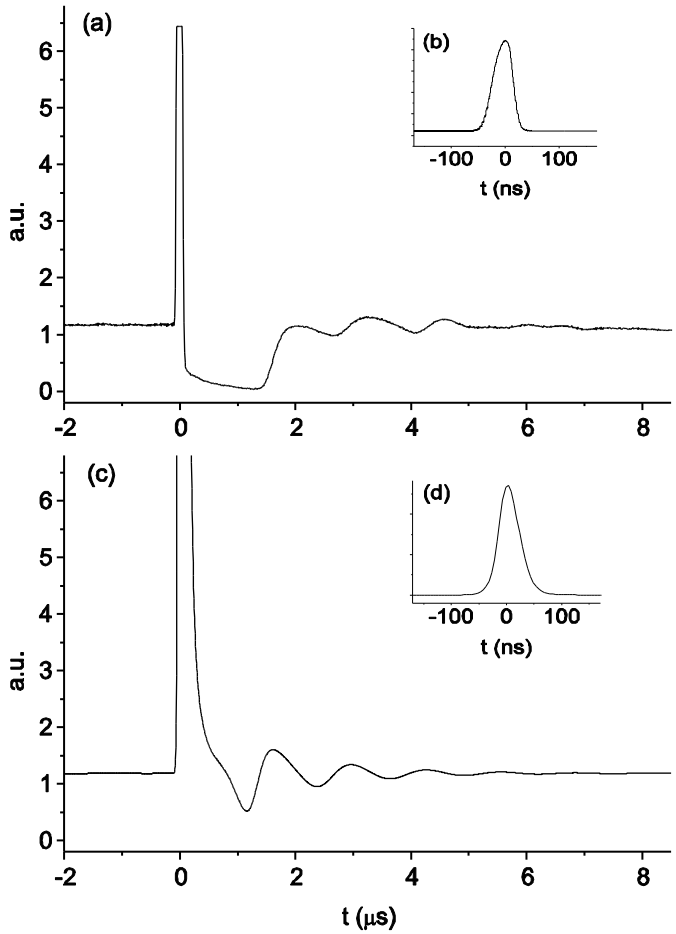

Fig. 2

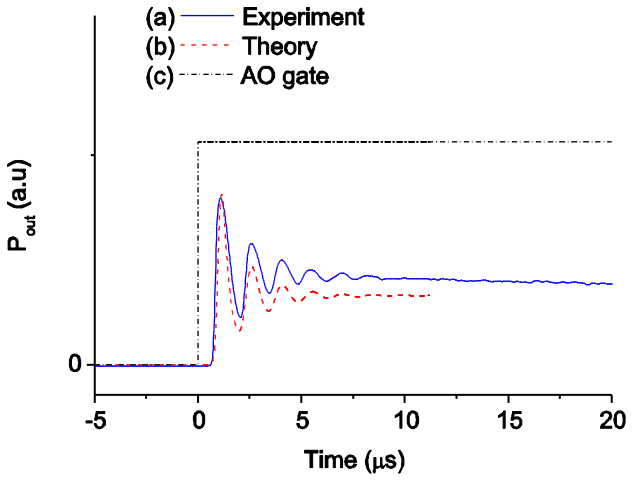

Fig. 3

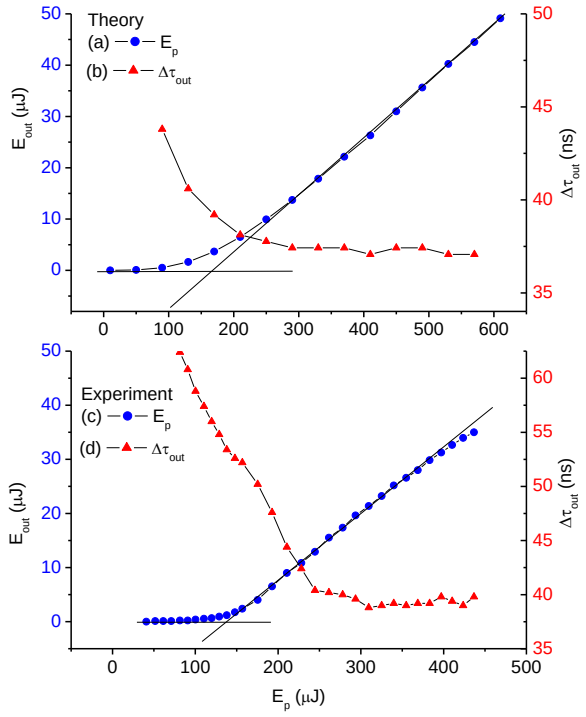
Theory
(a) E_p
(b) Δτ_out
E_out (μJ)
Δτ_out (ns)
Experiment
(c) E_p
(d) Δτ_out
E_p (μJ)

Fig. 4

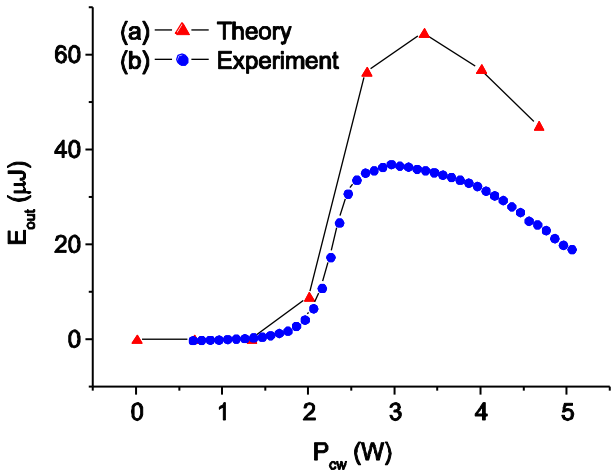

Fig. 5

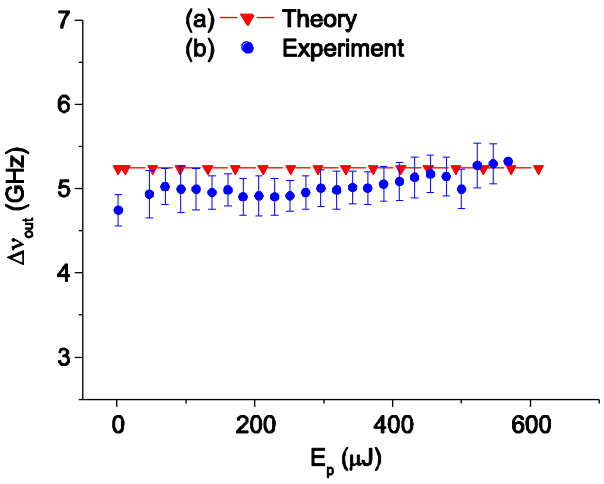
(a) Theory
(b) Experiment
7
6
5
4
3
$\Delta\nu_{out}$ (GHz)
0
200
400
600
E_p (μJ)

Fig. 6

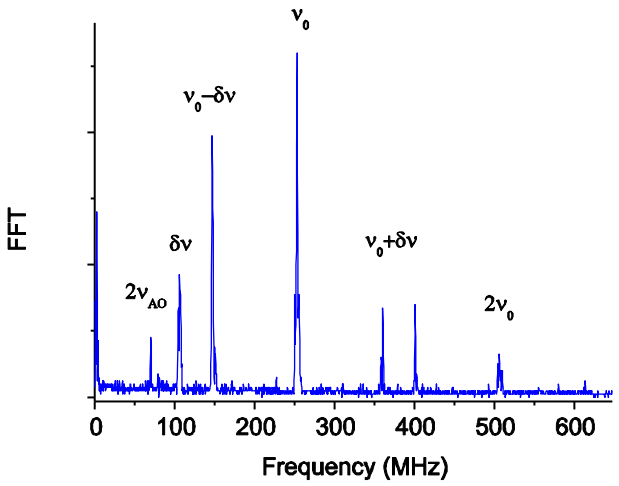
FFT
Frequency (MHz)
0
100
200
300
400
500
600
ν_0
$\nu_0-\delta\nu$
$\delta\nu$
$2\nu_{AO}$
$\nu_0+\delta\nu$
$2\nu_0$

Fig. 7